Thin Solid Films 769 (2023) 139738

Contents lists available at ScienceDirect

Thin Solid Films

journal homepage: www.elsevier.com/locate/tsf

Comparison of modified molecules 3-aminopropyltriethoxysilane and 11-aminoundecyltriethoxysilane in orientation angle and interaction with protein by sum frequency vibration spectrum and imaging ellipsometry biosensor

Haoyu Liu [a,b], Gang Jin [a,b,c,*]

[a] NML, Chinese Academy of Sciences, Institute of Mechanics, 15 Bei-si-huan West Road, Beijing 100190, China
[b] School of Engineering Sciences, University of Chinese Academy of Sciences, 19 Yu-quan Road, Beijing 100049, China
[c] School of Fundamental Physics and Mathematical Sciences, Hangzhou Institute for Advanced Study, University of Chinese Academy of Sciences, No.1, Sub-Lane Xiangshan, Xihu District, Hangzhou 310024, China

ARTICLE INFO

Keywords:
Aminosilane
Surface modification
Molecular orientation angle, Specificity, Immune globulin, Imaging ellipsometry biosensor
Sum frequency vibration spectrum

ABSTRACT

3-Aminopropyltriethoxysilane (APTES) has been widely used in biosensing as a surface-modifying molecule that acts as a bridge. The orientation and structure of APTES at the interface are major factors that affect biosensing efficiency. IgG (immunoglobulin G) is the most used and one of the most abundant immune proteins in the serum. We not only used broadband sum frequency generation vibrational spectroscopy to compare the spectrum of APTES and 11-aminoundecyltriethoxysilane (AUTES) molecules modified on a Si (111) surface but also compared the number and sensitivity of IgG adhered on APTES and AUTES surfaces by the imaging ellipsometry biosensor. We first found that the terminal amino groups of the APTES molecule were disorderly arranged by Sum frequency vibration spectrum (SFVS). Then we compared the performance of IgG immobilization in APTES or AUTES surfaces by imaging ellipsometry biosensor (IEB). In IEB, the anti-IgG detection LOD (limit of detection) on the APTES-modified surface(51 ng/mL) was higher than that on the AUTES-modified surface(380 ng/mL). We explored the relationship between the stability of aminosilane and the stability of biomolecules, and provided a reference for the selection of surface modification methods using aminosilane as a self-assembled membrane.

1. Introduction

With the development of fast and highly sensitive biosensors, the demand for attaching ligands to the surface of a variety of substrate materials is increasing [1–4]. Silicon has been widely used in biosensors as a substrate material [5,6]. However, silicon exposed to air spontaneously oxidizes to form a thin film of silicon dioxide, resulting in the complexity of uniformly fixing biomolecules (proteins, antibodies, etc.) on the silicon surface [7]. Therefore, a suitable silicon surface modification technology is needed to carry out biomolecule immobilization, which is one of the key steps in producing high-quality biosensors.

There are many surface modification methods on silicon surfaces, the most important of which is covalent fixation. The method of covalently fixing an organosilane self-assembling layer on a silicon surface [8] is a technology with great potential, and it has many advantages compared to other methods [5,6,9,10]. At present, it is generally believed that the self-assembly process of organosilane mainly includes the hydrolysis of silane groups and the formation of Si-O-Si bonds. First, the hydrolysis of the silane group results in the formation of reactive silanol groups. The hydrolyzed -Si-OH forms a hydrogen bond with the -OH on the Si substrate and then forms a strong Si-O-Si bond through the dehydration process [11–15], which provides many applications for the development of biosensors [14]. In fact, the adhesion of the ligand to the silicon surface depends critically on the structure and orientation of the organosilane self-assembled monolayer with a top reactive group (e.g., an amino group), which is a bridge used to connect with the ligand [16–18]. Simultaneously, the stability of the organosilane layer is important because it undergoes a series of biological processes, so any changes in this layer will greatly affect the performance of the biosensor. Therefore, it is very important to choose an appropriate organosilane as

* Corresponding author at: NML, Chinese Academy of Sciences, Institute of Mechanics, 15 Bei-si-huan West Road, Beijing 100190, China.
E-mail address: gajin@imech.ac.cn (G. Jin).

https://doi.org/10.1016/j.tsf.2023.139738
Received 3 October 2022; Received in revised form 8 February 2023; Accepted 13 February 2023
Available online 19 February 2023

the substrate modification molecule.

3-Aminopropyltriethoxysilane (APTES), a commonly used substrate modification molecule [19–23], is widely used to fix biomolecules on silicon surfaces [24–35]. Howarter et al. [36] studied the structure and morphology of APTES by atomic force microscopy by altering the reaction temperature, solution concentration, and reaction time. Three basic APTES morphologies were observed: a smooth film, a smooth thick film, and a rough thick film. Using these variables, the morphology and composition of the film can be controlled. Gunda et al. [37] studied the effects of APTES solution concentration and silanization time on the formation of a silane layer by FTIR (Fourier Transform Infrared) and modified the existing method of using APTES to form silane on a silicon substrate to produce a thin and stable silane layer for uniformly fixing biomolecules. Majoul et al. [38] studied the specific bands associated with Si-Si-H and O-Si-H groups of the APTES layer modified on the surface of porous silicon by FTIR spectroscopy, indicating that the functionalization of APTES can be evaluated by tracking the gradual decrease of the IR (tunable infrared) absorption peak intensity of the Si-Si-H and O-Si-H bands. Chabal et al. [39] compared the stability of APTES and long-chain 11-aminoundecyltriethoxysilane (AUTES) in PBS buffer solution using ellipsometric bias, indicating that short-chain APTES is not stable enough for biosensing applications. In contrast, long-chain SAMs (self-assembled layers) show higher stability and can be reproducibly grafted. These findings are the basis for the reliable preparation and stable operation of biosensors. However, the mechanism of more stable long-chain molecules is not explained microscopically. In addition, the structure of amino silane is the focus of the surface modification research field, but the relationship between the structure of amino silane and biomolecules has been ignored. This relationship not only determines the adsorption efficiency of biomolecular but also influenced the detection sensitivity of a biosensor.

An imaging ellipsometry biosensor (IEB) is a kind of optical biosensor that transforms the interaction of ligand and target into the optical signal (grayscale) in an image [40]. On the one hand, by combining ellipsometry with an imaging system (microscopy and a charge-coupled device (CCD)), IEB is capable of visualizing the variation in thickness of the sensing surface with a large field of view to several square centimeters and a high vertical spatial resolution better than 0.1 nm [41]. On the other hand, by introducing a microfluidic system, IEB has the advantage of detecting biomolecules with high throughput, sensitivity, specificity, and low sample consumption [42]. IEB has been applied to image and quantify various analytes, such as antibodies, pathogenic viruses, disease biomarkers, and bacteria [43]. Various covalent immobilization modification methods have been utilized in IEB to capture ligands [44]. However, the surface modification method needs to be optimized so that the surface can capture more ligands to improve the sensing signal.

Sum frequency vibration spectrum (SFVS) is a technique that provides molecular interface information by measuring the second-order nonlinear polarizability of a sample. For example, the orientation, arrangement, conformation, and kinetic parameters [45–49] of surface molecules can be obtained by the second-order nonlinear polarizability. To date, various interfaces have been analyzed by SFVS, such as simple molecular interfaces (water or ethyl alcohol), organic film interfaces (organic metal), macromolecule interfaces, and colloidal particle interfaces. In their research of aminosilane, Khuat et al. [50] for the first time used a nonlinear second-order surface SFVS instead of a linear IR spectrum to characterize the structure of APTES modified on a Si (111) substrate. However, the spectral resolution was low, and no obvious symmetrical dependence of the spectrum on the rotation angle was observed.

In this work, we not only used broadband SFVS to study the arrangement and terminal amino group orientation of APTES and AUTES molecules modified on Si (111) substrates but also investigated their performance in protein immobilization on surfaces by IEB. We obtained the Si (111) -APTES/AUTES spectrum via different polarization combinations and rotation angles. The results showed that the alignment and orientation of the amino groups in AUTES are more orderly than those in APTES. Moreover, the number and sensitivity of a protein (IgG) adhered on APTES or AUTES-modified surfaces were detected by IEB. Although the number of proteins adhered on the AUTES-modified surface was greater than that on the APTES-modified surface, the sensitivity of proteins on the APTES-modified surface was more than on the AUTES-modified surface. This study not only explained the reason for the stability of aminosilane from the microscopic view (the number of groups) but also provided a reference in the field of biosensing surface in surface modification from the macroscopic consequence (the number of adsorbed protein).

2. Experimental details

2.1. Materials and reagents

Polished silicon wafers from General Research Institute for Nonferrous Metals (Beijing, China) were used for the substrate of the IEB. 3-Aminopropyltriethoxysilane (APTES), glutaraldehyde (GLU), human immunoglobulin (IgG) from serum, anti-Human IgG antibody (anti-IgG), bovine serum albumin (BSA) and Phosphate buffered saline (containing 0.05% Tween-20, pH 7.4, PBST) were purchased from Sigma-Aldrich. The 11-Aminoundecyltriethoxysilane (AUTES) was purchased from Alfa Aesar. Ultrapure water was obtained from a MILLI-Q® EQ 7000 Ultrapure Water Purification System (18.2 mΩ at 25 °C) and used to prepare all the solutions.

2.2. Apparatus and detection principles of IEB

The IEB is composed of an imaging ellipsometry system and a microfluidic microarray bioreactor. In the imaging ellipsometry section, the configuration of the light path is based on the standard ellipsometry configuration of the polarizer-compensator-sample-analyzer (PCSA). The specific light path composition is shown in Fig. 1(a). The light beam from the Xe lamp is extended and collimated toward the polarizer. Beyond the polarizer, the linearly polarized light beam passes through a compensator (quarter wave plate) and impinges on the sensing surface. After reflection, the light beam passes through a second polarizer, called the analyzer, and strikes the CCD.

As we demonstrated in our previous work [44] and schematically illustrated in Fig. 1, under optimized conditions the grayscale response correlated approximately linearly to the surface mass density variation of the protein layer with a relative error of less than 0.2%. The relationship between the IEB signal, δ_I, and the surface mass density of the protein layer, $\delta\Gamma$, can be given by [44]

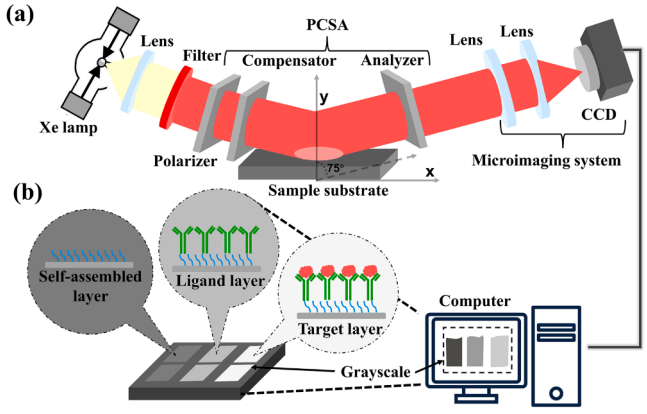

Fig. 1. The IEB for the detection of protein. (a) Schematic of IEB with the typical conventional PCSA. (b) The bioreaction process on the sensing surface and the procedure of the detection of protein by IEB.

$$\delta I \propto \delta\Gamma = \delta\gamma \cdot M \quad (1)$$

where δγ and M are the surface amount density of the protein layer and the protein molecular weight, respectively. Therefore, the different grayscales represent the different surface mass densities of different protein layers. As shown in Fig. 1(b), the ligand adsorbs on the SAMs by covalent interactions, and the target adsorbs on the ligand by affinity interactions, which increases the surface mass density. The increasing surface mass density would show in an increasing grayscale. As a result, surface adsorption can be deduced by grayscale. All the imaging ellipsometry experiments were performed at an incidence angle of 75° with a xenon lamp and a red optical filter.

As shown in Fig. 2, the microfluidic microarray bioreactor makes up of 24 polydimethylsiloxanes (PDMS) rectangle well arrays (Fig. 2(a)), polymethyl methacrylate, 48 microtubes (Fig. 2(b)), and a peristaltic pump. The peristaltic pump delivers the sample solution to the bioreactor. Each well of the PDMS plate has an area of 1 mm × 3 mm, a depth of 3 mm, resulting in a cell volume of 9 μL. Each well is connected through two 1-mm holes to two ends of 0.8 mm inner diameter, 1 mm outer diameter microtubes for performing the experiments. Twenty-four reaction cells are formed by inserting a modified Si plate. The sample solutions that are allowed to flow into the array of 24 independent reaction cells react with the modified Si surfaces of these cells as described in Section 2.6

2.3. Spectroscopic ellipsometry

The aminosilane layer thickness was estimated by spectroscopic ellipsometry (SE, J.A. Woollam Co. RC2-D, USA) using different incident angles (55°, 60°, 65°, 70°, 75°). Three irradiation sources were used: a 30 W deuterium lamp, a 20 W quartz tungsten halogen lamp, and a 75 W Xenon lamp in the spectral range of 193–1000 nm.

Thickness and MSE of the base self-assembled layer, of the ligand added layer, and of the target adsorbed layer on it were obtained from SE data fitting using CopleteEASE® software. The SE data analysis process begins by building two films layered optical model which corresponds to the nominal sample structure as shown in Fig. 3. In this experiment, silicon dioxide layer is film 1 and aminosilane layer is the film 2. Each layer is parameterized by thickness and optical constants. Optical constants describe how light interacts with and propagates through the layer. Using the Si with thermal oxide model and standard textbook thin film equations (Snell's law and Fresnel equations), the software can calculate "generated" or simulated SE data. If the model is a good representation of the sample, the model-generated SE data will be in good agreement with the SE data measured on the sample.

2.4. Detection principles of SFVS

SFVS is based on the generating frequency of light. As shown in Fig. 4 (a), when a fixed-frequency beam of visible light and an infrared light

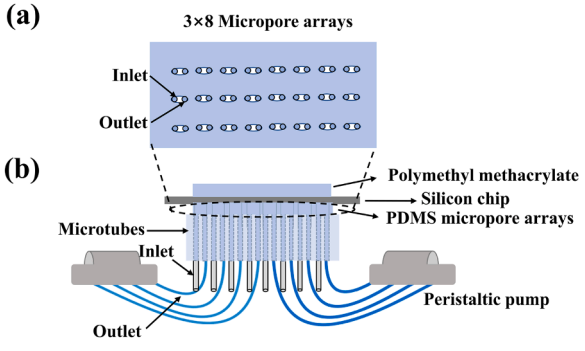

Fig. 2. Schematic of the (a) microarray with 24 cells, (b) microfluidic microarray bioreactor.

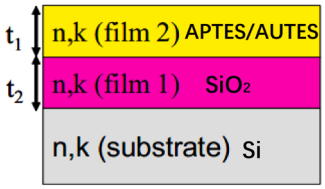

Fig. 3. Schematic representation of a layered optical model with 2 films, parameterized by thicknesses t_1 and t_2, and optical constants refractive index (n) & reflectivity (k).

act together at the molecular interface coincident with time and space, a frequency of light (harmony frequency signal) is generated. The harmonic frequency signal is enhanced when the interface produces resonance that results from a matched IR frequency and interfacial molecule vibration level. It is then detected by a spectrometer (SpectraPro HRS-500) and CCD (Andor). Therefore, the structure of molecules on the interface can be determined by adjusting the spectrum of infrared light frequency changes or vibrations. The Nd: YAG (Neodymium-doped Yttrium Aluminium Garnet; Nd: $Y_3Al_5O_{12}$) laser device (5.6 W power, 31 fs pulse width, and 1 kHz repetition frequency) is divided into two beams. One is 800 nm visible light (10 mW). The other is the adjustable infrared light range of 1000–4000 cm^{-1} produced by the OPA (optical parametric amplification) and DFG (digital function generator) systems. The specific light path diagram has been detailed in Liu et al. article [51].

The defined axis system in the SFVS is shown in Fig. 4(b). In the laboratory-fixed axis system (X, Y, Z), the Z-axis is the surface normal, and the X-Z plane is the incident plane of Vis (visible light) and IR (infrared light). The incident angles of Vis and IR are 45° and 55°, respectively. The Si-(111) is placed on a rotating platform. SFVS is generated by the coincidence of Vis and IR on the surface of the Si-(111) substrate. SFVS, Vis, and IR are P-, P- and P-polarization (PPP) or S-, S- and P-polarization (SSP) combinations, respectively. The azimuth is defined as the angle between the $[1\bar{1}0]$ crystal orientation of the Si-(111) substrate and the incident plane. In the experiment, samples were rotated at 30° intervals within an azimuth range from 0° to 360°, and the spectra of Si-(111) and Si-(111) –sample surfaces were collected at different azimuths.

The SFVS fitting results were found using equations. The fitting equations are as follows:

$$I_{SF}(\omega_{IR}) = \left| A_{NR} + \sum_v \frac{A_v e^{i\phi_v}}{\omega_{IR} - \omega_v + i\Gamma_v} \right|^2 \times \left(\sum_n a_n exp\left[-\frac{(\omega_{IR} - \omega_n)^2}{2\tau_n^2} \right] \right) \quad (2)$$

where a_n, ω_n, and τ_n are the amplitude, angular frequency, and bandwidth of the n-th Gaussian function, respectively, and A_v, ω_v, and Γ_v are the amplitude, angular frequency, and bandwidth of the Lorentzian function for a vibrational mode, v, respectively. ϕ_v represents the phase difference between the resonance response and the non-resonance response. Assuming that the non-resonance response is constant, it can be expressed as A_{NR}.

2.5. Silicon surface modification

All silicon surfaces were cleaned in piranha solution (H_2SO_4/H_2O_2 = 3:1, v/v) for 30 min, and then washed with deionized water several times. According to the different solvents required in next experiments, the silicon surface is treated as follows.

2.5.1. Ethanol treatment

After being washed with ethanol three times, the silicon surfaces were immersed in an ethanol solution of APTES (15:1, v: v) or AUTES (15:1, v: v) with densely packed amino groups for 2 h. After rinsing in

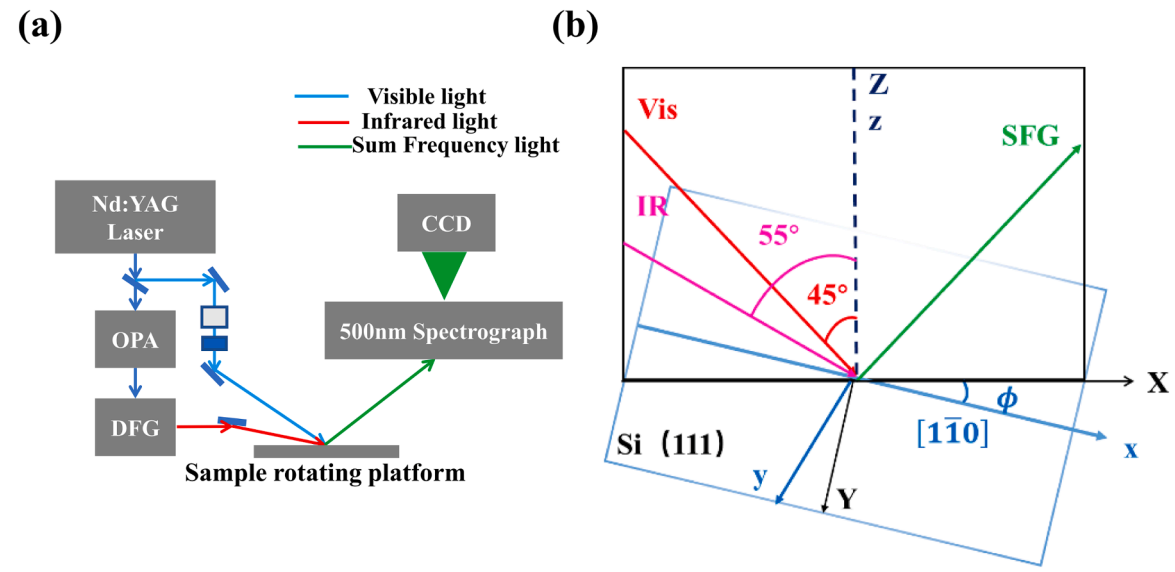

Fig. 4. SFVS simple light path and coordinate system. (a) Simplified schematic diagram of the SFVS device, (b) definition of the laboratory coordinate system and sample surface coordinate system. The azimuth (ϕ) is defined as the angle between the [1$\bar{1}$0] crystal orientation of the Si-(111) substrate and the incident surface.

ethanol, the surfaces were incubated in PBS of GLU (10:1, v: v) solution for 1 h. The silicon surfaces were stored at 4 °C after rinsing with PBS.

2.5.2. Toluene treatment

The silicon surface was washed with toluene three times and immersed in a toluene solution of APTES (50:1, v: v) or AUTES (50:1, v: v) for 24 h. After rinsing in toluene, the surfaces were blown dry with nitrogen.

2.5.3. Temperature treatment

Surfaces were heated in Electro- a thermostatic blast oven (DHG-9053A) at 100 °C for 1 h.

2.6. Procedure of protein adsorption by the microfluidic microarray bioreactor

All biomolecules were delivered by a microfluidic microarray bioreactor in IEB. The specific parameters were set as follows: IgG was first covalently immobilized on the modified silicon substrate at 0.5 μL/min for 15 min, followed by washing with PBST. Then, blocking buffer BSA was injected at 0.5 μL/min for 15 min to block the nonspecific binding sites that did not immobilize the IgG on the surface, followed by washing with PBST. After that, anti-IgG was delivered at 0.5 μL/min for 15 min, followed by PBST for 5 min. The area of the reaction cell is 1 mm × 3 mm. The thickness of PDMS micropore arrays is 3 mm.

2.7. Sensitivity

The sensitivity study included establishing the calibration curve and evaluating the LOD. The calibration curve was performed to detect anti-IgG samples from 10 ng/mL to 1 μg/mL. The calibration curve was obtained by assaying each concentration at least 3 times. According to the International Union of Pure and Applied Chemistry definition, the LOD of the sensing signal is equal to 3S/ε, where S is the blank standard deviation ($n = 15$) and ε is the slope of the calibration curve.

3. Results and discussion

3.1. Thicknesses of AUTES and APTES modified on Si surfaces

To explore the relationship between the carbon chain length of aminosilane and the protein molecule, it is necessary to confirm the topography of aminosilane immobilized on the surface. We selected three parameters to reflect the topography of aminosilane on the surface: thickness, altitude distribution, and orientation. The SE and SFVS were, respectively used to quantify the thickness, altitude distribution, and orientation.

First, the saturation adsorption concentrations of AUTES and APTES were determined. Considering that the saturated adsorption concentration of APTES had been verified in previous work [14], we only just investigated the saturated adsorption concentration of AUTES. Silicon surface-modified APTES ethanol and AUTES ethanol were detected by SE. As shown in Table 1, the thickness of AUTES was 1.797±0.004 nm, and the thickness of APTES was 0.527±0.048 nm. Actually, the AUTES molecule has a longer carbon chain length than APTES, which means AUTES has a higher surface mass density than APTES when there is the same number of aminosilanes on the surface. Considering that the detection area has the same dimension, more surface mass density is reflected in a greater thickness. Therefore, the thickness of AUTES modified on the surface is larger than the thickness of APTES. This result is consistent with the theory.

3.2. Structure and amino orientation of AUTES and APTES modified on Si surfaces

Then, surface-modified AUTES and APTES were analyzed by SFVS. The C—H and N—H stretching frequency regions of APTES and AUTES are shown in Fig. 5. As shown in Fig. 5, four peaks were observed at 2851, 2875,2924, and 2964 cm^{-1}. These peaks were from the -CH_2- symmetric vibration (CH_{2ss}), the -CH_3 symmetric vibration (CH_{3ss}), the -CH_3 Fermi resonance (CH_3FR) and the -CH_3 asymmetric vibration

Table 1
SE results of the silicon surface modified in APTES/AUTES.

Type of film	Ψ (Psi,°)	Δ (Delta,°)	Thickness (nm)	MSE
Si (after washing with H_2O_2 &H_2SO_4)	5.120 ±0.010	12.640 ±0.020	–	–
APTES	1.933 ±0.048	50.255 ±0.691	0.527 ±0.003	3.421
AUTES	2.694 ±0.046	50.857 ±0.474	1.797 ±0.004	3.811

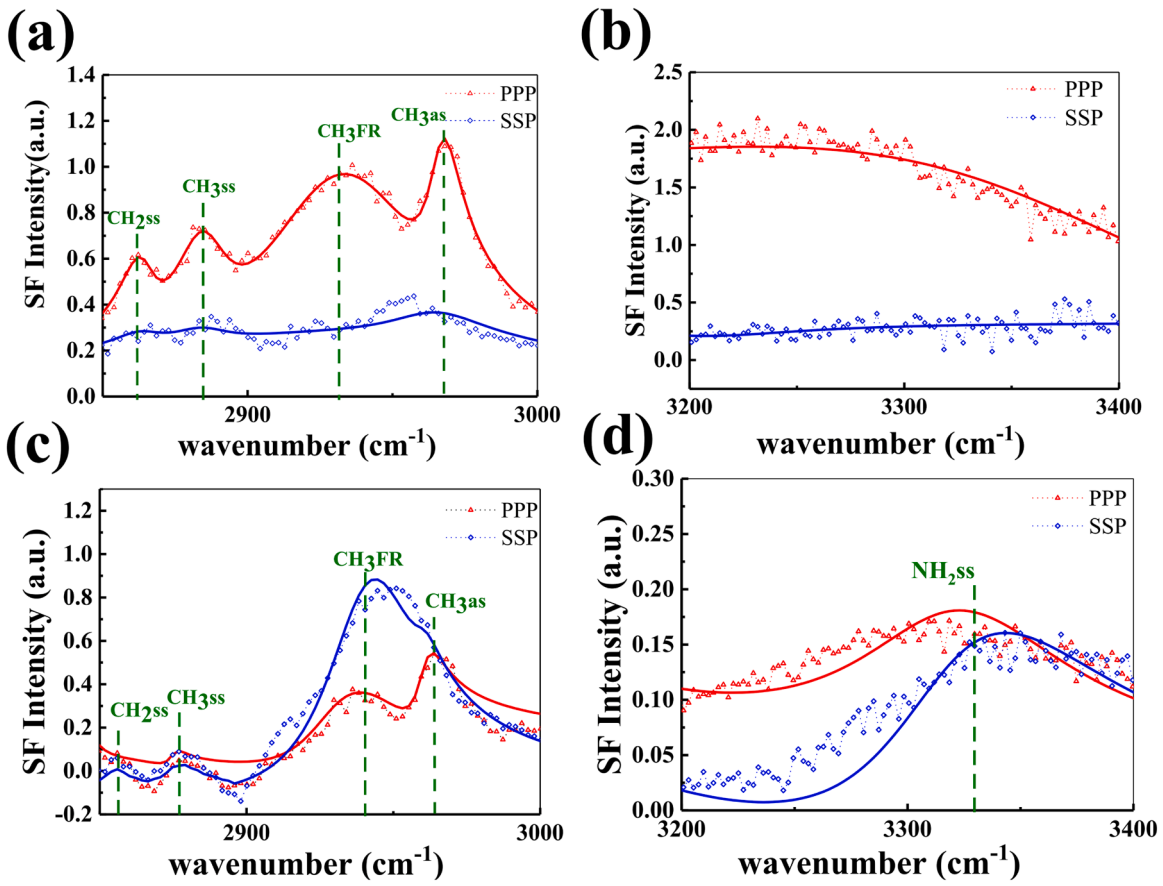

Fig. 5. SFVS spectra in the C—H and N—H stretching frequency regions of Si-(111) -APTES/AUTES at $\phi = 60°$ under PPP (red triangle) and SSP (blue diamond) polarizations. The solid line is the fitting result. (a) C—H region, Si-(111)-APTES, (b) N—H region, Si-(111)-APTES, (c) C—H region, Si-(111)-AUTES, (d) N—H region, Si-(111)-AUTES.

(CH_{3as}). These results indicated that not all ethoxy groups in APTES had been hydrolyzed in the reaction of modifying APTES to the silicon surface. As shown in Fig. 5(b), the SFVS spectrum in the N—H stretching frequency region of Si-(111) -APTES was fitted. There was no apparent amino vibration peak in the spectrum. However, since the amino molecules were buried by the upper molecules or because of the disorder of the amino orientation, a broad envelope appeared in the spectrum of the PPP polarization.

The SFVS spectra in the C—H and N—H stretching frequency regions of the Si (111) -AUTES spectrum at $\phi = 60°$ are shown in Fig. 5(c) and (d). As shown in Fig. 5(c), four peaks were observed at 2846, 2875, 2930 and 2960 cm^{-1}. These peaks represent the CH_{2ss}, CH_{3ss}, Fermi resonance CH_3FR, and CH_{3as}, respectively. These results indicated that the unhydrolyzed ethoxy chains in AUTES are arranged in a more orderly manner. This may be induced by the strong van der Waals force of the undecyl chain in AUTES. In addition, the N—H stretching frequency region of Si-(111) -AUTES is shown in Fig. 5(d). The peak at 3319 cm^{-1} is related to the -NH_2 symmetrical stretching vibration peak (NH_{2ss}). This indicates that some ethoxy groups were also not hydrolyzed during the reaction of modifying AUTES to the Si (111) surface.

In conclusion, the structure of AUTES was more ordered than that of APTES. On the one hand, the anti-symmetric vibrational peak of -CH_3 was redshifted by 4 cm^{-1}, which indicated that the unhydrolyzed ethoxy chains in AUTES were more orderly than those in APTES because of the strong van der Waals force of the undecyl chain among AUTES. On the other hand, the -NH_2 in AUTES had a vibration peak which suggested that the amino group in AUTES was more likely to be exposed on the surface than the amino in APTES.

3.3. The effects of solution and temperature in APTES immobilization

Ref. [52] showed that by curing the sample at room temperature or high temperature (100 °C) for a period of time, the upper molecules of the sample can be removed. Therefore, we heated the samples in DHG-9053A at 100 °C for 1 h before performing the SE measurement. As shown in Table 2, the thickness of APTES after heating was thinner than that at room temperature both in the ethanol solution or the methylbenzene solution. The thickness of the APTES in methylbenzene solution before and after heating was 4.44 nm and 2.17 nm, respectively. The thickness of the APTES layer in ethanol solution before and after heating was 1.61 nm and 1.29 nm, respectively. The thickness of the APTES monolayer obtained by the calculation was approximately 1.05 nm, so the hypothesis that the upper molecules buried the amino group can be ruled out. Therefore, it is concluded that no obvious amino group was observed because of the terminal amino group alignment disorder. In biosensors, the disorder of the terminal amino groups of APTES does not guarantee the connection of ligands, which will greatly reduce the binding efficiency of ligands and target molecules.

Table 2
SE results of the silicon surface modified in APTES in different conditions.

Layer	Solvent	Indoor temperature	Heating in 100 °C for 1h
Si modified with APTES	Methylbenzene	4.44±0.3 nm	2.17±0.3 nm
	Ethyl alcohol	1.61±0.3 nm	1.29±0.3 nm

3.4. The enhancement number of IGG by GLU

In fact, aminosilane usually combines with GLU to adsorb proteins (ligands) on silicon surfaces. GLU can enhance protein adsorption on the aminosilane-modified surface. In this section, the surface modified with APTES and the surface modified with APTES+ GLU and IgG adsorbed at three different concentrations detected by IEB.

First, three concentrations of IgG were prepared (1 μg/mL, 10 μg/mL and 100 μg/mL) in PBS. Then, IgG was delivered to the sensing surfaces modified with APTES or APTES+GLU by a bioreactor. Finally, the surfaces were placed on a IEB sample substrate and detected by IEB. As shown in Fig. 6, the lift Y-axis is the IEB signal of IgG layer. The right Y-axis is the variation signal of IgG layer ((Layer $_{IgG}$ - Layer$_{APTES+GLU}$) / Layer$_{APTES+GLU}$). The grayscale of IgG adhered on surface modified with APTES+GLU (red) had a higher grayscale than the surface modified with APTES (blue). Furthermore, the variation of IgG layer in APTES+GLU surface was twice or more than APTES surface (10 μg/mL or 100 μg/mL). But the variation of IgG layer is the same when the IgG concentration is 5 μg/mL. As shown in the Eq.. (1), a higher variation of IEB signal indicated a higher surface mass density. Therefore, the surface-modified APTES +GLU immobilized more IgG than the surface-modified APTES alone. GLU plays a role in increasing the number of IgG on aminosilane surfaces.

In fact, IgG is composed of many kinds of amino acids. There were two major kinds of chemical groups in the amino acid sequence: the carboxy group and the amino group. In particular, amino acid residues had more amino groups than carboxyl groups. Therefore, the surface modified with aldehyde groups (APTES+GLU) would adhere more IgG than amino groups (APTES). In other words, the number of IgG adhered on the sensing surface would be improved if the aldehyde group (GLU) was attached to the aminosilane molecule (APTES or AUTES). In all subsequent experiments, if there is no special mention, the surface covalent modifications are called APTES+GLU-modified surface and AUTES+GLU-modified surface.

3.5. The number of ligands adsorbed on the APTES and AUTES-modified surfaces

Although the structure of APTES and AUTES had discussed in Section 3.1. But it is unknown the relationship between the structure of aminosilane and adhered proteins. Therefore, APTES and AUTES surfaces adhered protein (IgG) were characterized by the IEB and SE, respectively.

Firstly, six concentrations of IgG (1 μg/mL, 2.5 μg/mL, 5 μg/mL, 10 μg/mL, 50 μg/mL, and 100 μg/mL) were detected by IEB. As shown in Fig. 7(a), the IEB signal variation of APTES+GLU surface was significantly higher than AUTES+GLU surface. As shown in Eq. (1), a higher variation of IEB signal indicated a higher surface mass density. Therefore, it can be assumed that the AUTES+GLU surface immobilized more IgG than the APTES+GLU surface between 1 μg/mL-100 μg/mL of IgG. In addition, it can be seen the IEB signal variation basically remains stable when the concentration of IgG ≥50 μg/mL. Considering signal maximization and saving the reagent consumption, 50 μg/mL IgG as ligand was used in next subsequent experiments. Then, the thickness of 50 μg/mL IgG adhered on AUTES/APTES+GLU surfaces was estimated by SE. As shown in Fig. 7(b), the thickness of IgG on AUTES+GLU was 1.430±0.03. But it's on APTES+GLU was 1.62±0.05. These results suggested that surface-modified AUTES would adhere to more proteins than surface-modified APTES. According to the inference of Section 3.2, the amino group in AUTES was more likely exposed on the surface than the amino in APTES. As a result, more sites on the surface-modified AUTES were provided to bind protein than surface-modified APTES.

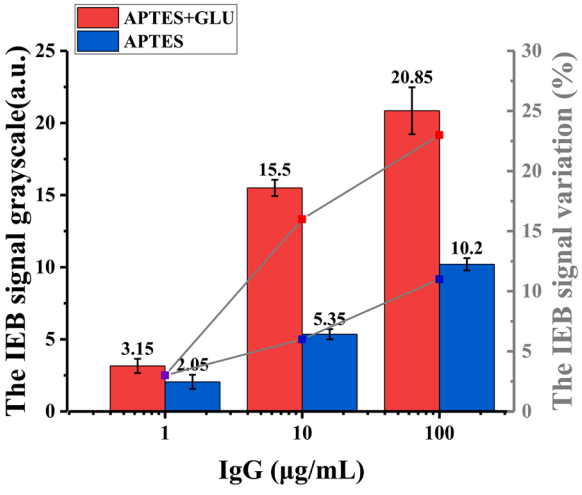

Fig. 6. The IEB signal (grayscale) or the IEB signal variation of IgG on APTES/APTES+GLU surfaces.

3.6. Sensitivity of target detection on APTES and AUTES-modified surfaces

In biosensor applications, target detection is the goal. However, the binding amount of the target depends on the sensitivity of the ligands. Therefore, it is necessary to compare the sensitivity of proteins (ligands) adhered to the APTES and AUTES surfaces. The sensitivity of the ligand is manifested in the degree of sensitivity interaction; that is, the number of antibodies is regarded as the ligand sensitivity parameter. The ligand in this experiment was still IgG. Therefore, the amount of anti-IgG bound IgG was considered the parameter of sensitivity.

In this part of the experiment, IgG (50 μg/mL) was used as a ligand, and five concentrations of anti-IgG (10 ng/mL, 50 ng/mL, 100 ng/mL, 500 ng/mL, and 1 μg/mL) were employed as targets. To avoid nonspecific adsorption, BSA (3 mg/mL) was used as a blocking buffer to block sites on the surface without IgG. First, the non-specific adsorption on APTES/AUTES-modified surfaces had been compared by IEB. As shown in Fig. 8, the grayscale of anti-IgG (negative) in APTES-modified surface was 1.53. But IgG on AUTES-modified surface had 2.38 grayscale. Theoretically, the lower non-specific signal had the higher positive signal of the specific signal. Therefore, the AUTES-modified surface has a higher positive signal rate than the APTES-modified surface.

The detection sensitivity of anti-IgG on APTES and AUTES-modified surfaces based on IEB was also analyzed. As shown in Fig. 9, the grayscale values of APTES (blue circles) were higher than the grayscale values of AUTES (red squares) surface at each concentration. As per Eq. (1), the surface mass density is directly proportional to the grayscale. Therefore, the number of anti-IgG on APTES was greater than that on AUTES. In addition, the slope of the calibration curve in APTES (0.0127 ±0.0008) was higher than the slope in AUTES (0.004175±0.00028). According to the LOD definition in the section "Sensitivity", the anti-IgG LOD on the AUTES-modified and APTES-modified surfaces were 380 ng/mL and 51 ng/mL, respectively. For anti-IgG concentrations ranging from 10 to 1000 ng/mL, the signal change of the APTES-modified surface reached about 13.4 grayscale and 4.32 grayscale for the AUTES-modified surface. The results show that the APTES-modified surface can detect anti-IgG effectively and obtain better analytical performance than the AUTES-modified surface. As the AUTES molecular arrangement is more orderly, more ligands can bound to it. However, once the number of ligands exceeds saturation, the ligand molecules overlap, covering specific sites, and resulting in decreased sensitivity [53]. Therefore, the surface sensitivity binding ability of AUTES-modified surfaces is lower than APTES-modified ones.

4. Conclusions

In this study, we not only used broadband SFVS to study the

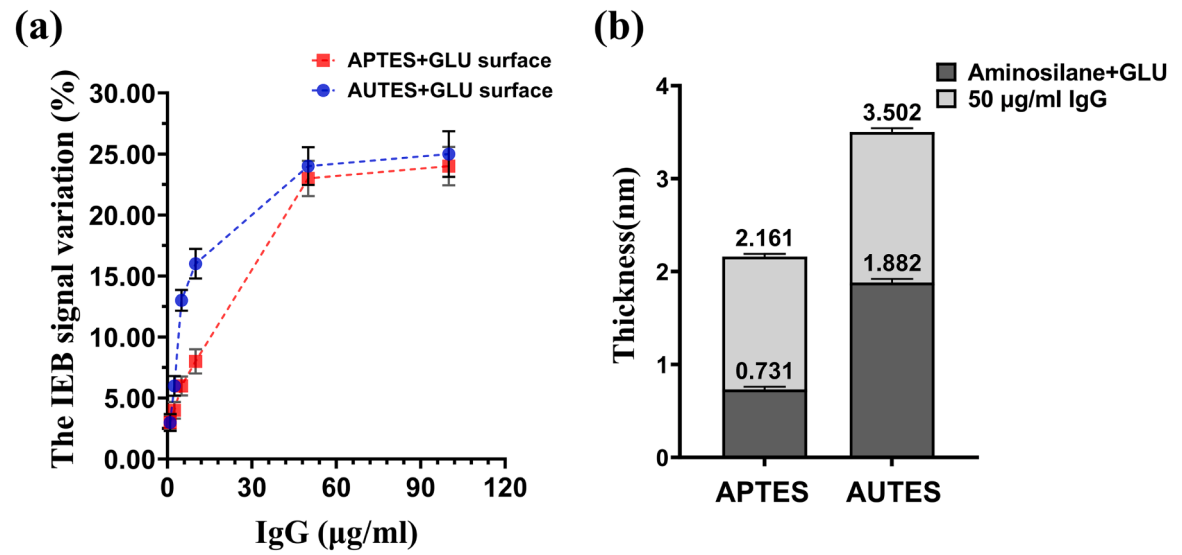

Fig. 7. Comparison of ligands surface mass density and thickness on the APTES and AUTES-modified surfaces. (a)The IEB signal variation at the concentration of 1 μg/mL, 2.5 μg/mL, 5 μg/mL, 10 μg/mL, 50 μg/mL, and 100 μg/mL IgG on APTES+GLU or AUTES+GLU-modified surfaces. (b)The thickness of different molecular film layer on APTES or AUTES modified surfaces.

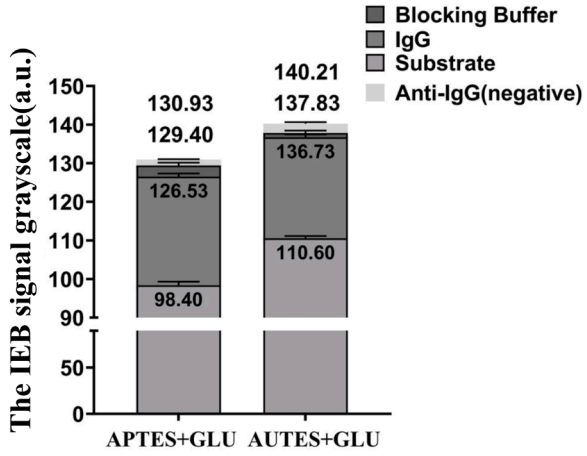

Fig. 8. The non-specific adsorption of anti-IgG(negative) detected by IEB.

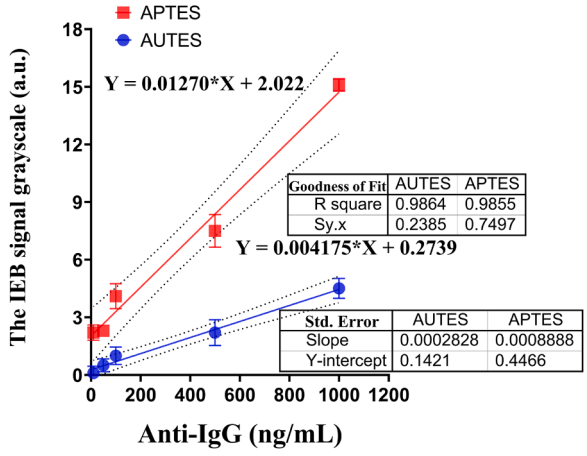

Fig. 9. The calibration curve for Anti-IgG detection on APTES or AUTES-modified surface by the IEB.

arrangement and terminal amino group orientation of APTES and AUTES molecules modified on Si (111) substrates but also investigated their performance in protein immobilization on the surface by IEB. The Si-(111) substrates were modified with APTES or AUTES. We analyzed and compared the alignment and orientation of the terminal amino groups in the two substrate-modified molecules. The results showed that the surface of silicon modified with AUTES was effective for regulating ligand orientation compared with that of APTES. However the IgG that adhered to APTES had more sensitivity. The APTES-modified surface had a higher LOD for the detection of anti-IgG than the AUTES-modified surface. Overall, the APTES-modified surface was more appropriate for application as a biosensor surface aminosilane modification molecule than AUTES. This work explored the relationship between the stability of aminosilane and the stability of biomolecules and provided a reference for the selection of surface modification methods using aminosilane as a self-assembled membrane.

CRediT authorship contribution statement

Haoyu Liu: Conceptualization, Methodology, Software, Visualization, Writing – original draft, Data curation. **Gang Jin:** Validation, Writing – review & editing, Resources, Supervision.

Declaration of Competing Interest

The authors declare that they have no known competing financial interests or personal relationships that could have appeared to influence the work reported in this paper.

Data availability

No data was used for the research described in the article.

Funding

This research did not receive any specific grant from funding agencies in the public, commercial, or not-for-profit sectors.

References

[1] Y. Cui, Q.Q. Wei, H.K. Park, C.M. Lieber, Nanowire nanosensors for highly sensitive and selective detection of biological and chemical species, Science 293 (2001) 1289–1292, https://doi.org/10.1126/science.1062711.

[2] E. Stern, J.F. Klemic, D.A. Routenberg, P.N. Wyrembak, D.B. Turner-Evans, A. D. Hamilton, D.A. LaVan, T.M. Fahmy, M.A. Reed, Label-free immunodetection with CMOS-compatible semiconducting nanowires, Nature 445 (2007) 519–522, https://doi.org/10.1038/nature05498.

[3] F. Patolsky, C.M. Lieber, Nanowire nanosensors, Mater. Today 8 (2005) 20–28, https://doi.org/10.1016/S1369-7021(05)00791-1.

[4] F. Patolsky, G.F. Zheng, C.M. Lieber, Nanowire-based biosensors, Anal. Chem. 78 (2006) 4260–4269, https://doi.org/10.1021/ac069419j.

[5] P. Jonkheijm, D. Weinrich, H. Schröder, C. Niemeyer, H. Waldmann, Chemical strategies for generating protein biochips, Angew. Chem. Int. Ed 47 (2008) 9618–9647, https://doi.org/10.1002/anie.200801711.

[6] F. Rusmini, Z. Zhong, J. Feijen, Protein immobilization strategies for protein biochips, Biomacromolecules 8 (2007) 1775–1789, https://doi.org/10.1021/bm061197b. Biomacromolecules.

[7] F. Tao, S. Bernasek, Functionalization of Semiconductor Surfaces, John Wiley & Sons, 2012. https://onlinelibrary.wiley.com/doi/book/10.1002/9781118199770.

[8] N. Glass, R. Tjeung, P. Chan, L. Yeo, J. Friend, Organosilane deposition for microfluidic applications, Biomicrofluidics 5 (2012) 1–7, https://doi.org/10.1063/1.3625605.

[9] J. Diao, D. Ren, J. Engstrom, K. Lee, A surface modification strategy on silicon nitride for developing biosensors, Anal. Biochem. 343 (2005) 322–328, https://doi.org/10.1016/j.ab.2005.05.010.

[10] J. Yakovleva, R. Davidsson, A. Lobanova, M. Bengtsson, S. Eremin, T. Laurell, J. Emnéus, Microfluidic enzyme immunoassay using silicon microchip with immobilized antibodies and chemiluminescence detection, Anal. Chem. 74 (2002) 2994–3004, https://doi.org/10.1021/ac015645b.

[11] M. Joshi, M. Goyal, R. Pinto, S. Mukherji, Characterization of anhydrous silanization and antibody immobilization on silicon dioxide surface, in: Proceedings of the IEEE International Workshop on Computer Architectures for Machine Perception, 2003, pp. 7–11, https://doi.org/10.1109/ISSMD.2004.1689550.

[12] R. Pasternack, S. Rivillon Amy, Y. Chabal, Attachment of 3-(aminopropyl) triethoxysilane on silicon oxide surfaces: dependence on solution temperature, Langmuir 24 (2008) 12963–12971, https://doi.org/10.1021/la8024827.

[13] Z.H. Wang, G. Jin, Silicon surface modification with a mixed silanes layer to immobilize proteins for biosensor with imaging ellipsometry, Colloids Surf. B Biointerfaces 34 (2004) 173–177, https://doi.org/10.1016/j.colsurfb.2003.12.012.

[14] N. Chaki, K. Vijayamohanan, Self-assembled monolayers as a tunable platform for biosensor applications, Biosens. Bioelectron. 17 (2002) 1–12, https://doi.org/10.1016/S0956-5663(01)00277-9.

[15] B. Arkles, P. Dispersants, Hydrophobicity, hydrophilicity and silanes, paint & coatings industry: serving liquid and powder manufacturers in the global marketplace 22 (2006) 114–135. https://www.gelest.com/wpcontent/uploads/HydrophobicityHydrophilicityandSilanes.pdf.

[16] N. Faucheux, R. Schweiss, K. Lutzow, C. Werner, T. Groth, Self-assembled monolayers with different terminating groups as model substrates for cell adhesion studies, Biomaterials 25 (2004) 2721–2730, https://doi.org/10.1016/j.biomaterials.2003.09.069.

[17] N.K. C.haki, K. Vijayamohanan, Self-assembled monolayers as a tunable platform for biosensor applications, Biosens. Bioelectron 17 (2002) 1–12, https://doi.org/10.1016/S0956-5663(01)00277-9.

[18] S.A. D.iBenedetto, A. Facchetti, M.A. R.atner, T.J. M.arks, Molecular self-assembled monolayers and multilayers for organic and unconventional inorganic thin-film transistor applications, Adv. Mater. 21 (2009) 1407–1433, https://doi.org/10.1002/adma.200803267.

[19] T. Vallant, J. Kattner, H. Brunner, U. Mayer, H. Hoffmann, Investigation of the formation and structure of self-assembled alkylsiloxane monolayers on silicon using *in situ* attenuated total reflection infrared spectroscopy, Langmuir 15 (1999) 5339–5346, https://doi.org/10.1021/la9900977.

[20] H. Tu, C.E. H.eitzman, P.V. Braun, Patterned poly(N-isopropylacrylamide) brushes on silica surfaces by microcontact printing followed by surface-initiated polymerization, Langmuir 20 (2004) 8313–8320, https://doi.org/10.1021/la049663a.

[21] Q. Weiping, X. Bin, W. Lei, W. Chunxiao, Y. Danfeng, Y. Fang, Y. Chunwei, W. Yu, Controlled site-directed assembly of antibodies by their oligosaccharide moieties onto APTES derivatized surfaces, J. Colloid Interface Sci. 214 (1999) 16–19, https://doi.org/10.1006/jcis.1999.6151.

[22] J. Landoulsi, M.J. Genet, K. El Kirat, C. Richard, S. Pulvin, P.G. Rouxhet, Silanization with APTES for controlling the interactions between stainless steel and biocomponents: reality vs expectation, Biomater. Phys. Chem. 5 (2011) 953–978. http://hdl.handle.net/2078.1/105272.

[23] N. Aissaoui, L. Bergaoui, J. Landoulsi, J. Lambert, S. Boujday, Silanes layers on silicon surfaces: mechanism of interaction, stability and influence on protein adsorption, Langmuir 28 (2012) 656–665, https://doi.org/10.1021/la2036778.

[24] S. Onclin, A. Mulder, J. Huskens, B.J. R.avoo, D.N. R.einhoudt, Molecular printboards: monolayers of β-cyclodextrins on silicon oxide surfaces, Langmuir 13 (2004) 5460–5466, https://doi.org/10.1021/la049561k.

[25] N. Lapin, Y. Chabal, Infrared characterization of biotinylated silicon oxide surfaces, surface stability, and specific attachment of streptavidin, J. Phys. Chem. B 113 (2009) 8776–8783, https://doi.org/10.1021/jp809096m.

[26] O. Seitz, P.G. Fernandes, R. Tian, N. Karnik, H.-.C. Wen, H. Stiegler, R.A. Chapman, E.M. Vogel, Y.J. Chabal, Control and stability of self-assembled monolayers under biosensing conditions, J. Mater. Chem. 21 (2011) 4384–4392, https://doi.org/10.1039/C1JM10132C.

[27] K.V. S.andeep, L. Edmond, H. Sabahudin, B.M. K.eith, H.T. J.ohn;, Immobilization of antibodies and enzymes on 3-aminopropyltriethoxysilane-functionalized bioanalytical platforms for biosensors and diagnostics, Chem. Rev. 114 (2014) 11083–11130, https://doi.org/10.1021/cr5000943.

[28] Q. Weiping, X. Bin, W. Lei, W. Chunxiao, S. Zengdong, Y. Danfeng, L. Zuhong, W. Yu, Orientation of antibodies on a 3-aminopropyltriethoxylsilane-modified silicon wafer surface, J. Inclusion Phenomena 35 (1999) 419–429, https://doi.org/10.1023/A:1008192209162.

[29] Q. Gu, X. Cheng, Tribological behaviors of self-assembled 3-aminopropyltriethoxysilane films on silicon, Curr. Appl. Phys. 8 (2008) 583–588, https://doi.org/10.1016/j.cap.2007.10.054.

[30] Y. Mo, M. Zhu, M. Bai, Preparation and nano/microtribological properties of perfluorododecanoic acid (PFDA)–3-aminopropyltriethoxysilane (APS) self-assembled dual-layer film deposited on silicon, Colloids Surf. A 322 (2008) 170–176, https://doi.org/10.1016/j.colsurfa.2008.03.004.

[31] J. Kim, P. Seidler, C. Fill, L.S. Wan, Investigations of the effect of curing conditions on the structure and stability of amino-functionalized organic films on silicon substrates by Fourier transform infrared spectroscopy, ellipsometry, and fluorescence microscopy, Surf. Sci. 602 (2008) 3323–3330, https://doi.org/10.1016/j.susc.2008.09.001.

[32] S.H. C.hoi, B.Z. Newby, Suppress polystyrene thin film dewetting by modifying substrate surface with aminopropyltriethoxysilane, Surf. Sci. 600 (2006) 1391–1404, https://doi.org/10.1016/j.susc.2006.01.050.

[33] R.M. P.asternack, S. Rivillon Amy, Y.J. C.habal, Attachment of 3-(Aminopropyl) triethoxysilane on silicon oxide surfaces: dependence on solution temperature, Langmuir 24 (2008) 12963–12971, https://doi.org/10.1021/la8024827.

[34] D.G. K.urth, T. Bein, Surface reactions on thin layers of silane coupling agents, Langmuir 9 (1993) 2965–2973, https://doi.org/10.1021/la00035a039.

[35] P.D.F. Siqueira, G. Wenz, P. Schunk, T. Schimmel, An improved method for the assembly of amino-terminated monolayers on SiO_2 and the vapor deposition of gold layers, Langmuir 15 (1999) 4520–4523, https://doi.org/10.1021/la981379u.

[36] J.A. H.owarter, J.P. Y.oungblood, Optimization of silica silanization by 3-aminopropyltriethoxysilane, Langmuir 22 (2006) 11142–11147, https://doi.org/10.1021/la061240g.

[37] N.S.K. Gunda, M. Singh, L. Norman, K. Kaur, S.K. M.itra, Optimization and characterization of biomolecule immobilization on silicon substrates using (3-aminopropyl)triethoxysilane (APTES) and glutaraldehyde linker, Appl. Surf. Sci. 305 (2014) 522–530, https://doi.org/10.1016/j.apsusc.2014.03.130.

[38] N. Majoul, A. Aouida, B. Bessais, Progress of porous silicon APTES-functionalization by FTIR investigations, Appl. Surf. Sci. 331 (2015) 388–391, https://doi.org/10.1016/j.apsusc.2015.01.107.

[39] O. Seitz, P.G. F.ernandes, R. Tian, N. Karnik, H.C. W.hen, H. Stiegler, Y.J. C.habal, Control and stability of self-assembled monolayers under biosensing conditions, J. Mater. Chem. 21 (2011) 4384–4392, https://doi.org/10.1039/C1JM10132C.

[40] G. Jin, R. Jansson, H. Arwin, Imaging ellipsometry revisited: developments for visualization of thin transparent layers on silicon substrates, Rev. Sci. Instrum. 67 (1996) 2930–2936, https://doi.org/10.1063/1.1147074.

[41] Y. Niu, G. Jin, Protein microarray biosensors based on imaging ellipsometry techniques and their applications, Protein Cell 2 (2011) 445–455, https://doi.org/10.1007/s13238-011-1054-x.

[42] Y. Chen, Y. Meng, G. Jin, Optimization of off-null ellipsometry for optical biosensor applications, IEEE (2006) 682–685, https://doi.org/10.1364/AO.46.008475.

[43] H. Liu, J. Shen, W. Liu, Y. Niu, G. Jin, Imaging ellipsometry biosensor: basic theory, principles of operation, and applications, J. Vac. Sci. Technol. B 38 (2) (2020), 024002, https://doi.org/10.1116/1.5129596.

[44] Y. Li, W. Liu, G. Jin, Y. Niu, Y. Chen, M. Xie, Label-Free sandwich imaging ellipsometry immunosensor for serological detection of procalcitonin, Anal. Chem. 90 (2018) 8002–8010, https://doi.org/10.1021/acs.analchem.8b00888.

[45] S.C. A.verett, A.R. C.alchera, J.E. P.atterson, Polarization and phase characteristics of nonresonant sum-frequency generation response from a silicon (111) surface, Opt Lett 40 (2015) 4879–4882, https://doi.org/10.1364/OL.40.004879.

[46] J. Kim, G.J. H.olinga, G.A. S.omorjai, Curing Induced Structural Reorganization and Enhanced Reactivity of Amino-Terminated Organic Thin Films on Solid Substrates: observations of Two Types of Chemically and Structurally Unique Amino Groups on the Surface, Langmuir 27 (2011) 5171–5175, https://doi.org/10.1021/la2007205.

[47] Y.R. S.hen, Phase-Sensitive Sum-Frequency Spectroscopy, Annu. Rev. Phys. Chem 64 (2013) 129–150, https://doi.org/10.1146/annurev-physchem-040412-110110.

[48] Y.R. S.hen, V. Ostroverkhov, Sum-frequency vibrational spectroscopy on water interfaces: polar orientation of water molecules at interfaces, Chem. Rev. 106 (2006) 1140–1154, https://doi.org/10.1021/cr040377d.

[49] S. Nihonyanagi, S. Yamaguchi, T. Tahara, Direct evidence for orientational flip-flop of water molecules at charged interfaces: a heterodyne-detected vibrational sum frequency generation study, J. Chem. Phys. 130 (2009), 204704, https://doi.org/10.1063/1.3135147.

[50] T.T.H. Khuat, L. Liang, T.T. P.han, G. Mizutani, H.N. Rutt, Sum frequency generation study of immobilized 3-aminopropyltriethoxysilane self-assembled layer on Si(111) substrates, Surf. Interface Anal. 51 (2019) 120–125, https://doi.org/10.1002/sia.6570.

[51] X.J. Liu, Xu S, Y.Q. Li, G. Jin, R.R. Feng, Sum-frequency spectrum phase measurement of the silica-octadecyl trichlorosilane interface and measurement

accuracy analysis, Spectrosc. Spectral Anal. 41 (2021) 789–795, https://doi.org/10.3964/j.issn.1000-0593 (2021)03-0789-07 (In Chinese).
[52] K. Joonyeong, J.H. George, A.S. Gabor, Curing induced structural reorganization and enhanced reactivity of amino-terminated organic thin films on solid substrates: observations of two types of chemically and structurally unique amino groups on the surface, Langmuir 27 (2011) 5171–5175, https://doi.org/10.1021/la2007205.
[53] Y. Niu, T. Kang, G. Jin, Joint detection of tumor markers with imaging ellipsometry biosensor, Thin Solid Films 571 (2014) 453–462.